Monte Carlo simulation of miniature endplate current generation in the vertebrate neuromuscular junction

Thomas M. Bartol Jr.,* Bruce R. Land,‡ Edwin E. Salpeter,§ Miriam M. Salpeter*

*Section of Neurobiology and Behavior, Division of Biological Sciences, Seeley G. Mudd Hall, Cornell University, Ithaca, New York 14853; ‡Cornell National Supercomputer Facility, Center for Theory and Simulation in Science and Engineering, Cornell University, Ithaca, New York 14853; and §Department of Physics, Cornell University, Ithaca, New York 14853 USA

ABSTRACT   A Monte Carlo method for modeling the neuromuscular junction is described in which the three-dimensional structure of the synapse can be specified. Complexities can be introduced into the acetylcholine kinetic model used with only a small increase in computing time. The Monte Carlo technique is shown to be superior to differential equation modeling methods (although less accurate) if a three-dimensional representation of synaptic geometry is desired. The conceptual development of the model is presented and the accuracy estimated. The consequences of manipulations such as varying the spacing of secondary synaptic folds or that between the release of multiple quantal packets of acetylcholine, are also presented. Increasing the spacing between folds increases peak current. Decreased spacing of adjacent quantal release sites increases the potentiation of peak current.

I. INTRODUCTION

The vertebrate neuromuscular junction (nmj) (see Fig. 1, a and b) is an ideal synapse for studying the events following the release of a quantal packet of transmitter (acetylcholine, ACh). The nmj can be easily voltage clamped to record the miniature endplate currents (MEPC's) that result from such a release. Furthermore, from experiments which record changes in MEPC shape (rise time, amplitude, and fall time) as a result of changing the nmj microenvironment (for instance, by changing acetylcholinesterase [AChE] and/or acetylcholine receptor [AChR] concentrations) one can derive some of the kinetic parameters of ACh interactions.
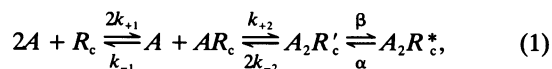
In previous publications (Land et al., 1980, 1981, 1984) such derivations were obtained by solving simultaneous differential equations for ACh diffusion, plus binding/unbinding to AChR. This treatment required simplifications in both the kinetic schemes and nmj geometry used in the model. The present paper describes the development and verification of a Monte Carlo simulation which allows us to follow the individual fate of every ACh molecule released into the cleft of a nmj, and do so for junctions whose geometry is more realistically portrayed. We first present validation tests for the model and then apply the method to determine the effect of varying endplate geometry and/or the distance between two ACh release sites. Comparison of computational cost and accuracy from a full and a simplified chemical kinetic scheme is also discussed.

Address all correspondence to Dr. Salpeter.

II. MONTE CARLO METHOD AND VALIDATION

A. Kinetic schemes and comparisons between differential equations and Monte Carlo simulations as a means of modeling

In addition to diffusion, the usual full kinetic scheme for ACh behavior in the primary cleft of the nmj can be expressed as:

$$2A + R_c \underset{k_{-1}}{\overset{2k_{+1}}{\rightleftharpoons}} A + AR_c \underset{2k_{-2}}{\overset{k_{+2}}{\rightleftharpoons}} A_2R'_c \underset{\alpha}{\overset{\beta}{\rightleftharpoons}} A_2R^*_c, \qquad (1)$$

where A is ACh; R_c is an AChR molecule containing 2 ACh binding sites plus a channel which can be either in a closed or open conformation; AR_c is the singly bound molecule, $A_2R'_c$ is the doubly bound molecule in the closed conformation, and $A_2R^*_c$ is the doubly bound molecule in the open conformation (Adams, 1975). To fully account for all the parameters when modeling MEPC's, one has to solve simultaneously the differential equations for ACh diffusion, binding/unbinding, and channel isomerization. In the past (Adams, 1975; Sheridan and Lester, 1977; Land et al., 1984) the standard scheme in Eq. 1 was often replaced by a simpler, approximate scheme:

$$2A + R_c \underset{k_{-1}}{\overset{2k_{+1}}{\rightleftharpoons}} A + AR_c \underset{\chi_{-eff}}{\overset{k_{+2}}{\rightleftharpoons}} A_2R_c, \qquad (2)$$
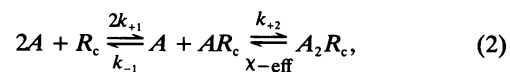
where $\chi_{-eff} \approx 2k_{-2}[\alpha/(\beta + \alpha)]$. In this scheme R_c and AR_c are the unbound and singly bound molecules, as in the full scheme, but only one doubly bound state A_2R_c is used, combining the kinetics for the $A_2R'_c$ and $A_2R^*_c$

steps. To obtain $A_2R_c^*$ in this approximation, A_2R_c must be multiplied by $\beta/(\beta + \alpha)$ which is the fraction of double bound receptor molecules that are in the open conformation, i.e., the quantity "g" in Land et al. (1981). The simplified approximate scheme can be used if the rate constants satisfy the inequality $k_{-2} \ll (\alpha + \beta)$. A comparison of the numerical accuracy of results from both schemes is discussed in section V.

Even more complicated schemes than given in Eq. 1 (not including desensitized states) have been postulated. For instance, it has been suggested (Sine and Taylor, 1980; Blount and Merlie, 1989; Hartman and Claudio, 1990) that the two binding sites on a receptor molecule have different binding kinetics, giving two nonequivalent singly bound AR_c states, and five possible states in all. There is also considerable evidence from patch-clamp studies of single-channel currents (e.g., Labarca et al., 1985) that in addition to the doubly liganded open state ($A_2R_c^*$), there may also be a singly liganded open state, making seven possible states for AChR. In addition, the presence of a possible third binding site with inhibitory properties has also been postulated (Udgaonkar and Hess, 1986) in which case future modeling may need to deal with up to 14 states for the receptor molecule and even more if one considers the possibility of channel openings from unliganded AChR. The implications of these more complex kinetic schemes for MEPC generation will be addressed in detail in a subsequent paper. However, we can foreshadow the effect which the inclusion of channel openings from singly liganded AChR's will have on the time course of a MEPC. Due to the initial high concentration of ACh no effect is expected during the rising phase of the MEPC. In principle there could be an effect at the later stages of the falling phase when few of the AChR molecules are doubly bound. With AChE intact the effect is expected to be small because of the rapid channel closings suggested by the single-channel experiments (Labarca et al., 1985). In situations where the AChE has been removed, single-channel openings would cause a very slowly decreasing "tail" to the falling phase.

Another cause for complexity in endplate modeling stems from variations in detailed geometry. The geometry of a neuromuscular junction differs from one animal species to another and for different muscle types within one species. In particular, some muscles have no secondary folds and in others the interfold spacing can vary (for review see Salpeter, 1987). For the case of a nmj without any secondary folds, where the receptor surface is a plane sheet, the diffusion can be approximated as two-dimensional because the cleft height is small compared with the distance over which a quantal packet spreads. Furthermore, since in that case there is radial

symmetry, one could reduce the spatial variables to a single variable, i.e., the one-dimensional distance "r" to the release site. Most previous modeling (Wathey et al., 1979; Land et al., 1981, 1984) used this one-dimensional approximation. However, for accurate modeling of cases with secondary folds, (see Fig. 2) one needs a calculation in a fully three-dimensional space.

It is useful at this point to contrast the two radically different computational approaches to modeling MEPC's numerically for a given geometry and assumed kinetic scheme. The first, using simultaneous coupled differential equations, characterizes the distribution of free ACh molecules by a density function of space and time, $A(x, y, z; t)$. This and other functions for the various states of the receptor complexes are solved numerically. Such a method was used previously by Land et al. (1981, 1984) and by Wathey et al. (1979) but only for the function $A(r; t)$ in the one-dimensional approximation. The second approach, using the "Monte Carlo method," first characterizes the distribution by specifying the position (x, y, z) for each of a number (N) of ACh molecules at a given time t (and the state of the receptor molecule if the ACh molecule is bound to it). In this method the time development of the distribution is achieved not by a differential equation, but by following each molecule in space and time as it diffuses.

The practical limitations of computational costs are very different in the two methods and depend on the complexity of the problem to be solved. Consider first free diffusion in the one-dimensional approximation. The pure diffusion equation for ACh concentration, A, in the absence of any chemical reactions would read:

$$d/dt\, A(r, t) = D(\partial^2 A/\partial r^2), \qquad (3)$$

where D is the diffusion coefficient, ∂ is the partial derivative, and r is radial distance. In the differential equation approach one approximates the continuous differential equation (Eq. 3) for the function $A(r, t)$ by a difference equation with finite (but small) increments Δr and Δt. A fundamental requirement of the difference equation method is that Δr and Δt be small enough so that the function $A(r, t)$ varies by only a small percentage from one value of r to the adjacent value, $r + \Delta r$ (similarly for time). The number (n_s) of r values at which the function $A(r)$ has to be evaluated is inversely proportional to Δr. Similarly the number of time steps (n_t) is inversely proportional to Δt. The difference equation method has the agreeable property that doubling n_s and n_t (when halving Δr and Δt) decreases the numerical error of the final results by much more than a factor of two (Ortega and Poole, 1981). High accuracy can thus be achieved. However, for a given distance analyzed, such as for a typical MEPC, n_s and n_t have to
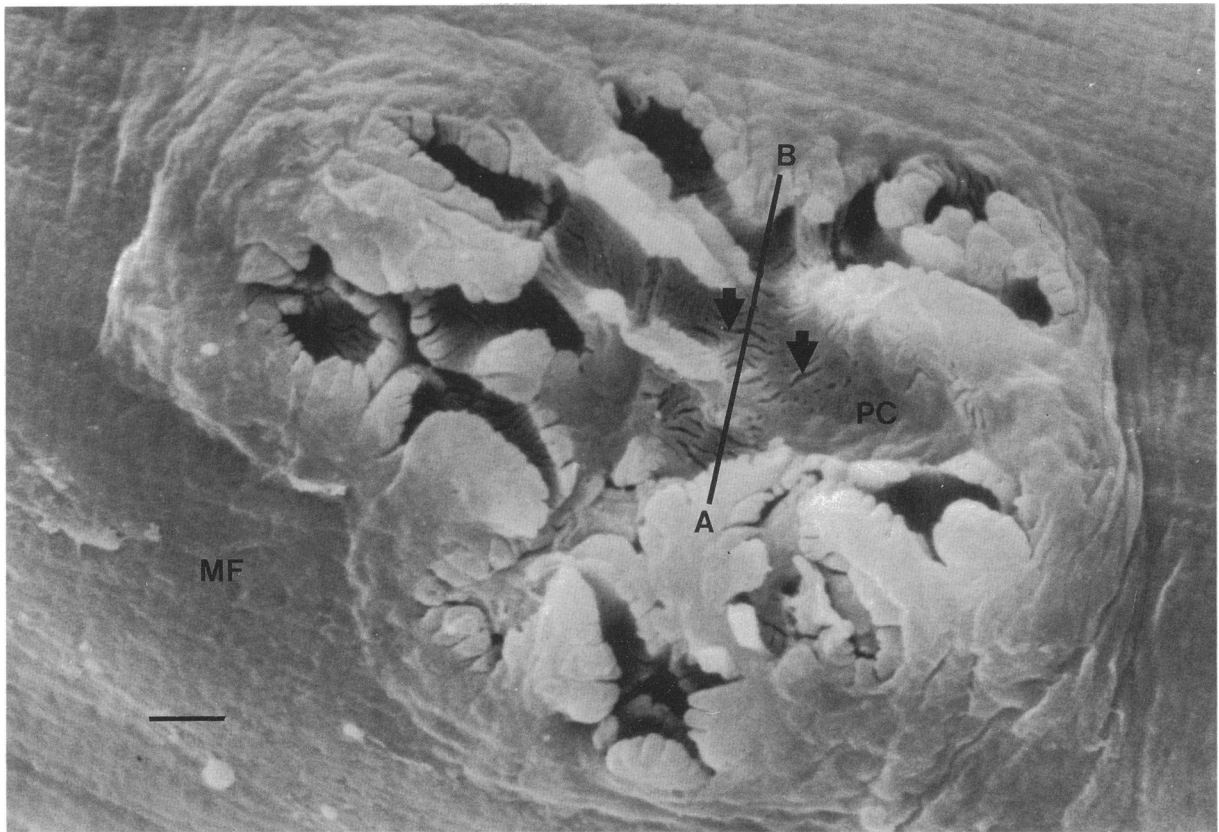
FIGURE 1 (*a, b*)   Scanning Electron Micrograph (SEM) (*a*) and Transmission Electron Micrograph (TEM) (*b*) of lizard intercostal muscle neuromuscular junction (nmj). (*a*) In this SEM of a lizard muscle fiber (MF), the presynaptic neuron has been removed to show the surface of the post-synaptic membrane. The primary cleft (PC) and secondary clefts (*arrows*) of the nmj can be seen. This micrograph illustrates the characteristic oval shape of the lizard nmj, similar to that of mammalian muscle. If a cross-section of the nmj is taken along line A-B the structures seen in *b* are exposed. Magnification ×6200, scale is 2.0 μm.

be fairly large, e.g., between 10^2 and 10^3 each. The number of operations required is then $\sim n_s n_t$ or $\sim 10^4$ to 10^6, which is feasible on modern computers. However, for a fully three-dimensional function of Cartesian space coordinates x, y, and z (plus time t), one still needs n_s different values for each of the three coordinates and the number of operations required is of order $n_s^3 n_t$ or $\sim 10^8$ to 10^{12}, which is extremely time consuming even for a modern supercomputer.

In the Monte Carlo method one does not deal with any density function, but follows the position of each of N molecules as a function of time, i.e., $r(t)$ for the one-dimensional case and three coordinates $x(t)$, $y(t)$, and $z(t)$ in the three dimensional case. The Monte Carlo method thus mimics the real life situation more exactly. To do the simulation, N is kept constant and a time step, Δt, is chosen during which a molecule is allowed to move in a straight line.

The time step, Δt, has to be small compared with the

time over which conditions change appreciably (e.g., the rise time, t_r, for a MEPC). As long as $t_r/\Delta t > 100$ then the choice of Δt does not introduce a major error in the Monte Carlo calculation (see section II B). Errors in the Monte Carlo method then come mainly from the finite number (N) of ACh molecules used for a quantal release. Because Poisson fluctuation are of the order $N^{1/2}$, the fractional errors are $\sim 1/N^{1/2}$ in an individual MEPC simulation. Because N is fixed, one can gain greater accuracy only by repeating the number of MEPC simulations "n" times and averaging the results. Repeating this calculation "n" times increases the computing cost by "n" but decreases fractional errors of the result by only $1/n^{1/2}$ just as in the case of repeating actual experiments (the final fractional error for "n" MEPC simulations is of order $1/[nN]^{1/2}$). Thus, increasing accuracy in the Monte Carlo method is not as easy as it is for the differential equation method. However, unlike the case with differential equations, going from a one-
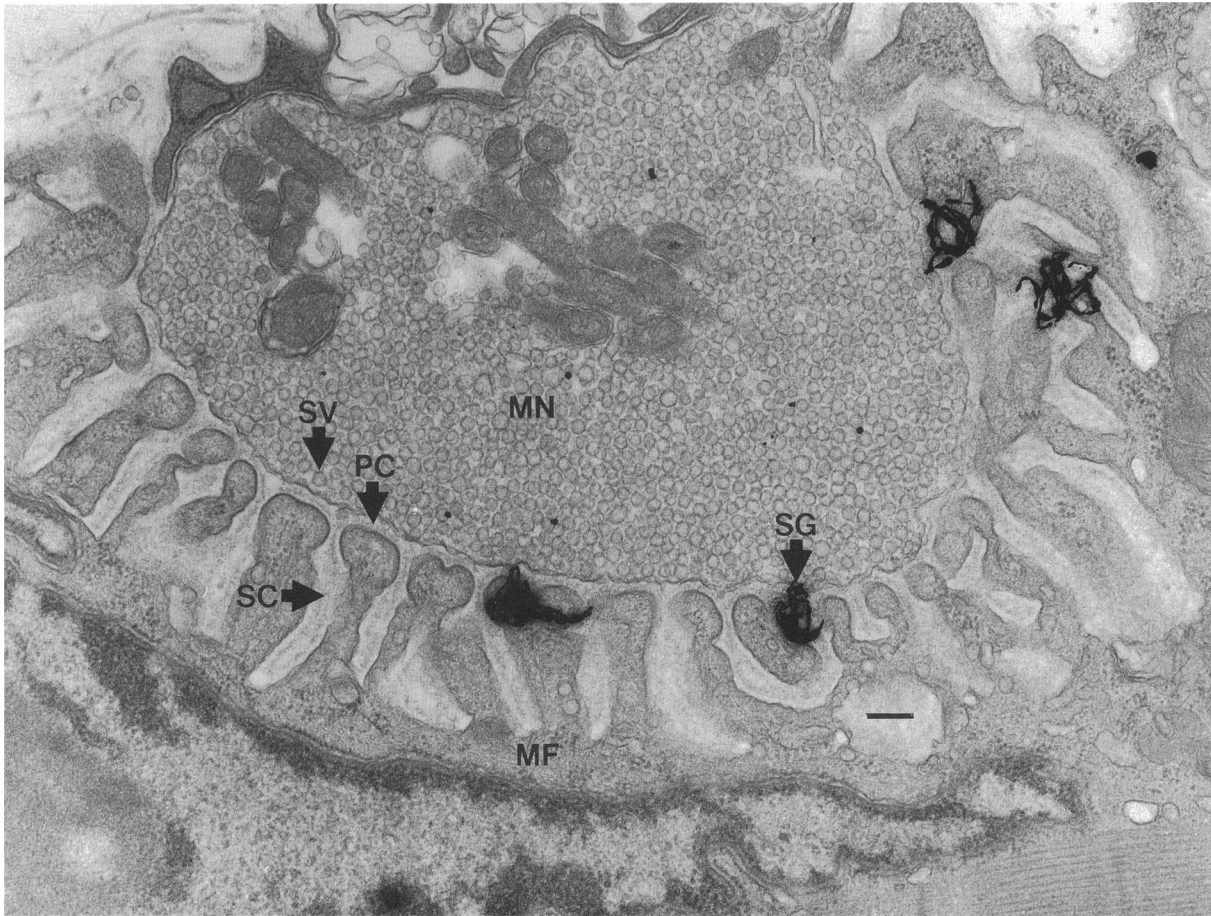
FIGURE 1 (continued) (*b*) TEM of a lizard nmj with the presynaptic motor-neuron (MN) intact showing much of the fine-structure of this nmj (see also Salpeter et al., 1984, Salpeter, 1987). Synaptic vesicles (SV) are tightly packed within the neuron. The acetylcholine receptors (AChR's), found mainly at the top ~ 250 nm of the folds formed by the primary (PC) and secondary (SC) clefts, are at a density of $\sim 8,200$ molecules per μm^2 of muscle membrane. In this TEM autoradiogram the AChR's are labeled with ^{125}I α-bungarotoxin localized by selective silver grains (SG). The acetylcholinesterases (AChE's) are associated with the basal lamina in both the primary and secondary clefts (Hall and Kelly, 1971; Betz and Sakmann, 1973; McMahan et al., 1978). Magnification $\times 33000$, scale is 0.2 μm.

dimensional to a three-dimensional calculation does not increase Monte Carlo computing costs greatly. It only involves keeping track of (and choosing random numbers for) three instead of one time-varying coordinate. Therefore, in the Monte Carlo method the computing cost in a three-dimensional calculation is only about three times larger than for the one-dimensional case, in contrast to the difference equation method where the computing cost is increased by a factor $\sim n_s^2 \geq 10^4$.

Similarly, in going to more complex kinetic schemes, the difference equation method becomes more difficult to solve as the number of equations used to describe the more complex kinetic scheme increase. Each new molecular state added to the kinetic scheme involves adding two more equations. The associated matrix of equations, therefore, grows to $(n + 2) \times (n + 2)$ and adds complexity to the method. In contrast (as will be seen in section V), adding a new molecular state to the Monte Carlo method as when going from Eq. 2 to Eq. 1 involves only adding another algorithm to the choices allowed for an ACh molecule, but does not change the diffusion routine or the total number of molecules, N. Because, as we shall see, the diffusion routine is the most time consuming part of a Monte Carlo routine, an increase in kinetic scheme complexity does not increase computer time appreciably.

To summarize the pro's and con's of the two methods: the differential equation method is preferable if the geometry and chemical kinetic scheme used are simple (one-dimensional approximation and simplified kinet-
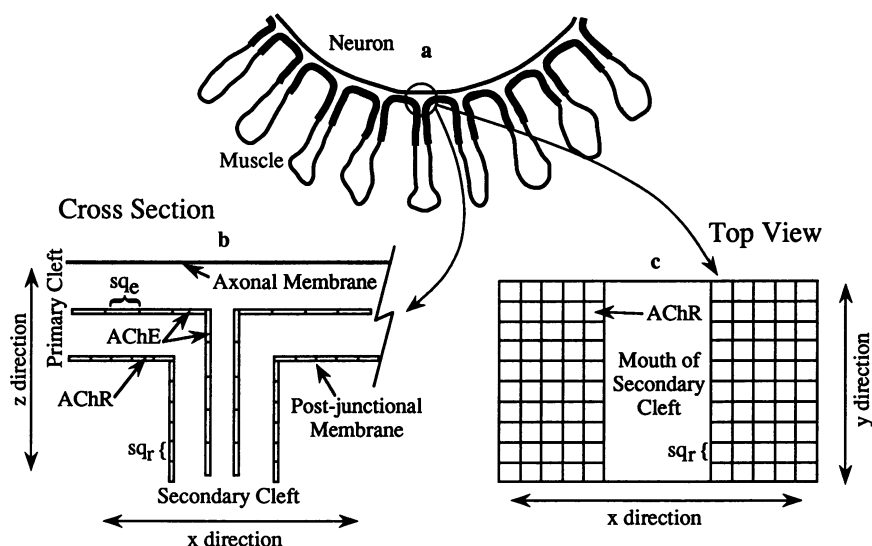
FIGURE 2 (a, b, c) Schematic views of real (a) and model (b, c) neuromuscular junction. (a) Line drawing of real nmj (see Fig. 1 b). AChR is indicated by thick line at top of junctional folds. Circle indicates area magnified in schematic of model nmj (b, c). (b) Cross-section of model nmj. Axonal and post-junctional membranes are the bounding surfaces. The axonal membrane is tiled with AChR (length of AChR tile is sq_r). AChE is located in lumen of primary and secondary cleft. Length of AChE tile is sq_e. A double layer of AChE is present in secondary cleft bounded by each of the junctional fold membranes. (c) Top view of model nmj. AChR tiles are shown covering surface of post-junctional membrane. AChE is not shown.

ics) and if great numerical accuracy is required. The Monte Carlo method is preferable (even essential, from a practical point of view) if one requires realistic modeling of geometry and chemical kinetics. Results with an accuracy of a few percent (e.g., for the peak MEPC amplitude) can be achieved fairly easily, but extremely great numerical accuracy is not a practical goal. Another advantage of the Monte Carlo method is the ability for visual presentations as will be seen below. Although the results of models using difference methods may also be visualized, the images obtained from a Monte Carlo simulation allow one to appreciate the highly stochastic nature of a process.

B. Steps in Monte Carlo simulations

Monte Carlo simulations in general have already been described by Rubinstein (1981). Applications to diffusion and chemical kinetics are discussed by Torney and Warnock (1988) and by Turner (1977). Below we describe only those points in the methodology which were used in modeling MEPC's for the nmj.

Before commencing a particular simulation, we specified the boundaries of the volume in terms of Cartesian coordinates (x, y, z) of the surfaces (membranes) within which the free ACh molecules are allowed to move but not cross. A number of parameters were also specified such as the densities of the AChR molecules (σ_r) (the

density of ACh binding sites is $\sigma_s = 2\sigma_r$) and of the AChE active sites (ACh binding sites, σ_e), the number (N) of ACh molecules per quantal packet, the diffusion constant (D), the chemical kinetic parameters for AChR (six if Eq. 1 is to be used, four if Eq. 2 is to be used, and more for more complex schemes), and the kinetic parameters for AChE (k_{+e} and k_{-e}). The values for σ_r and σ_e are taken from experimental measurements. However N, D, and the chemical kinetic parameters were allowed to vary as will be discussed in a future paper.

Finally, we specified a "Monte Carlo time step" Δt, at the end of which each ACh molecule is "interrogated" as to its activity during this period (i.e., distance and direction moved, the new location and the state of binding, as described below). For a given value of Δt and the diffusion constant, D, the average distance moved in any Cartesian coordinate is given by the net diffusion length (L_d) defined by

$$L_d^2 = 4D(\Delta t/\pi).$$ (4)

Diffusion theory (Crank, 1975) gives the probability of moving some distance between ($L - \Delta L$) to ($L + \Delta L$), for any value of L. This probability is proportional to the area under the diffusion distribution function (the error function) between ($L - \Delta L$) and ($L + \Delta L$). We chose 100 successive bins in the diffusion distribution function

with equal probability of occurring. Since each bin with midpoint L_j ($j = 1$ to 100) has equal area, the bin width and thus the spacing, $L_{j+1} - L_j$, varies. Explicitly:

$$L_j = L_d \pi^{1/2} \, \mathrm{erf}^{-1}(j/100 - 0.5/100), \qquad (5)$$

where erf^{-1} is the inverse error function (van der Laan and Temme, 1984). The properties of the erf^{-1} function are such that the average value of L_j is L_d (as required), the median value, L_{50} is ~ 0.84 times L_d, and the largest L_j value is $L_{100} \sim 3.6 \, L_d$. Each Cartesian coordinate, ($x, y,$ and z separately) is then either increased or decreased (randomly) by a distance L_j, determined by choosing j from a uniform random number generating routine and substituting into Eq. 5.

The computing cost for a MEPC simulation is inversely proportional to the time step Δt. It would obviously be too costly to mimic the actual Brownian motion of molecules (with $\Delta t < 10^{-3}$ μs). However, Δt must be small compared with the time over which bulk conditions change appreciably; i.e., $\Delta t \ll t_r$, where t_r is the 20% to 80% rise time of a MEPC (~ 100 μs). We found that $\Delta t < 0.02 t_r$ is sufficiently small not to cause any appreciable errors, as checked by comparing results from two simulations carried out with two different values of Δt. During the falling phase of a MEPC conditions change more slowly than during the rising phase and one could increase Δt after the peak amplitude is reached. However, for ease in Monte Carlo bookkeeping, we introduced an additional constraint and required that the largest of the 100 step lengths ($\sim 3.6 \, L_d$) be less than twice the cleft height, Z (therefore, for $2Z \sim 100$ nm, $L_d \leq 27$ nm). For instance, for free diffusion $D \sim 6 \times 10^{-6} \mathrm{cm}^2\mathrm{s}^{-1}$ (Eccles and Jaeger, 1958; Krnjevic and Mitchell, 1960; Dionne, 1976; Wathey et al., 1979), and rearranging Eq. 4 gives $\Delta t \sim (27 \, \mathrm{nm})^2/(6 \times 10^{-6} \mathrm{cm}^2\mathrm{s}^{-1})$, so that we generally use $\Delta t \leq 1$ μs.

In an actual computation, the AChR molecules on the postsynaptic membrane surface are modeled as small squares of length sq_r (Fig. 2) each having 2 ACh binding sites (for the lizard we used $sq_r = 11$ nm). Thus, $1/sq_r^2 = \sigma_r$, is the density of the AChR molecules. After each Δt time step, when an ACh molecule has moved a distance L_j, (determined as described above), the ACh molecule is interrogated as follows: the line joining the old and new position of the ACh molecule is examined. If the molecule had hit (crossed) any bounding surface where there is no AChR (e.g., the surface is an axonal membrane or is at the bottom of the folds) or if the molecule hit an AChR which is already fully bound with 2 ACh molecules then specular reflection is specified, (i.e., the particle is still allowed to move as originally specified in the two dimensions parallel to the surface,

but its direction perpendicular to the surface after the hit is reversed and it is thus bounced off the hit surface). If, on the other hand, the ACh molecule had hit an AChR square that has a free ACh binding site, the computer chooses a random number between 0.0 and 1.0 (to nine decimal places). If this random number is less than a predetermined fractional number p_+ (see below) the ACh molecule is allowed to bind; if the random number lay between p_+ and unity specular reflection without binding is again specified and the ACh molecule bounces off the surface.

The number p_+, i.e., the "Monte Carlo binding probability per time step Δt", has to be related to the forward binding rate constant, k_+, defined by chemical kinetics. To do this we consider that if A is the concentration (in molarity) of free ACh in the volume above the surface, chemical kinetics requires the binding rate per AChR square to equal $(k_+)(A)\mathrm{s}^{-1}$. Since, in the Monte Carlo simulation, the average of all diffusion step lengths L_j is L_d, half of all the ACh molecules which are within a perpendicular distance L_d of the receptive surface will, on the average, hit during one time interval Δt. Thus the number of ACh molecules that hit per AChR square per Δt is: $0.5 \, N_a A$, (where A is the molar concentration of ACh within that volume and N_a is Avogadro's number) times $L_d sq_r^2$ (i.e., the volume above the AChR square). This number of hits times the probability p_+ of binding gives the number of bindings per time step which must equal $k_+ A \Delta t$, thus relating p_+ to k_+. Using $sq_r^2 = 1/\sigma_r$ and Eq. 4 for L_d, Eq. 6 a gives this relation in two alternative forms:

$$p_+ = (k_+/N_a)\sigma_r(\pi \Delta t/D)^{1/2} = p_{+0}(L_d/sq_r), \qquad (6a)$$

where p_{+0}, the Monte Carlo binding probability for the special step length $L_d = sq_r$, is given by:

$$p_{+0} = (k_+/N_a)(\pi/2Dsq_r). \qquad (6b)$$

Of course, Δt and L_d have to be chosen small enough so that $p_+ < 1$. For typical values of k_+ for ACh to AChR binding $p_{+0} \ll 1$ so that we can choose L_d several times sq_r and still have $p_+ < 1$.

If a molecule is bound to a receptor, its chemical kinetic rate constant k_- for unbinding likewise has to be converted to a "Monte Carlo probability" p_- for unbinding. Per time step, $p_- = 1 - \exp(-k_- \Delta t)$, which is close to $k_- \Delta t$ as long as $k_- \Delta t$ is small compared with 1. To determine whether a molecule unbinds during a time step we again randomly choose a number between 0 and 1, and allow unbinding if it is between 0 and p_- and retain binding if it is between p_- and 1. Upon unbinding, an ACh molecule is moved an average step length (L_d) from the AChR to which it had been bound. In actual

simulations one has to make a distinction between singly bound and doubly bound AChR complexes with a corresponding suffix 1or 2 for $p_\pm$ and $k_\pm$.

There are many more AChR squares on the receptive surfaces than there are ACh molecules released in a single quantal packet, but in our bookkeeping we need to keep track of only individual ACh molecules. After each time step the position (x, y, z) of each ACh molecule is determined and whether it is bound to an AChE site or to an AChR (singly or doubly) is noted. The procedure followed for AChE binding is described below. The possibility of a free ACh molecule exiting from the cleft is also considered. In our previous numerical calculations (Land et al., 1984) we defined the boundary at which a diffusing ACh molecule is lost from the cleft as a circle on the primary cleft membrane of radius R_{ex}. In our current model, however, it is more convenient to define a square or rectangular region with sides $2X_{ex}$ and $2Y_{ex}$ in the x and y directions, respectively (instead of a circle with diameter $2R_{ex}$). The x direction was defined as that along the long axis of the muscle, whereas the y direction is at 90° to the x axis and in the plane of the membrane. The quantal packet release site can be anywhere in the rectangle; if an ACh molecule diffuses outside the rectangle it is removed from the simulation.

For hydrolysis by an AChE active site we use a simplified chemical kinetic scheme with only two parameters: we choose a value for the binding rate constant k_{+e} between ACh and AChE sites and define a probability p_{+e} by analogy with Eq. 6

$$p_{+e} = 1/2(k_{+e}/N_a)\sigma_e(\pi\Delta t/D)^{1/2}. \tag{7}$$

In this equation the factor ½ corrects for the fact that because the AChE is assumed to be in the basal lamina in the middle of the cleft (Hall and Kelly, 1971; Betz and Sakmann, 1973; McMahan et al., 1978) it can be hit by molecules moving up as well as those moving down, and the AChE active site density, σ_e, replaces σ_r. We then simplify the hydrolysis by a single hydrolysis/unbinding rate constant k_{-e} ($\sim 3{,}600$ s^{-1}) (Vigny et al., 1978) and use a probability $p_{-e} = k_{-e} \Delta t$ per time step for the AChE active site becoming free again and (simultaneously) the ACh being destroyed irreversibly.

When the full chemical kinetic scheme in Eq. 1 is used (see section V), we have an additional isomerization routine: if a doubly bound AChR is in the closed state (A_2R_c') we use a probability $p_{+i} = 1 - \exp(-\beta\Delta t) \sim \beta\Delta t$ per time step for switching to the open state $(A_2R_c^*)$ and a probability $p_{-i} \sim \alpha\Delta t$ for the inverse process. In all our runs both p_{-i} and p_{+i} were <0.02. A similar routine would be used if one postulated singly liganded open channels.

C. Validation tests

To validate our model, test cases were chosen for which analytical solutions could be computed accurately and the results compared with the model output. This was done for the diffusion, collision, binding, and unbinding segments of the computer program. Due to the complexity of our model it was necessary to break the testing procedure into several steps.

1. Diffusion

We tested the diffusion of 5,000 ACh molecules (equivalent to a small quantal packet) so that the percentage fluctuations would be the maximum to be seen after normal quantal release. Two conditions were tested:

(a) The first diffusion test involved diffusion in open space with no reflecting walls: initially all ACh molecules start at the same point in space (from a point source) and are then allowed to diffuse for a certain number of iterations T. At the end of T time steps the radial distribution of particles away from the original starting point is computed. For this simple case, the expected density distribution is known analytically: the volume density $A(r, t)$ as a function of radial distance r from the source at time t, should be:

$$A(r, t) = N_0(4\pi t D)^{-3/2} \exp(-r^2/4tD), \tag{8}$$

where D is the diffusion constant, N_0 is the total number of molecules released and $r = (x^2 + y^2 + z^2)^{1/2}$ is the three-dimensional radial distance from the origin. This analytic function A, is plotted in Fig. 3 against the radial distance, r, expressed in micrometers. The experimental points in Fig. 3 were obtained from the Monte Carlo simulation, and represent the number N_j of molecules in successive bins r_j to $r_j + \Delta r$ divided by $4\pi r_j^2\Delta r$, (the volume of each bin) to give ACh concentration. The error bars denote the "Poisson fluctuation" $\pm (N_j^{1/2}/4\pi r_j^2 \Delta r)$, i.e., the expected deviations from a smooth curve due to the finite number of molecules.

Fig. 3 shows excellent agreement with expectations, but also illustrates an intrinsic limitation of any Monte Carlo method: because $N \propto 4\pi r^2$, the fractional error $(N_j)^{-1/2}$ is large when r is small, i.e., near the origin. This situation does not improve even after many time steps. Fortunately, most practical results of the simulation, e.g., rise time and amplitude of a MEPC represent averages over many adjacent spatial bins.

(b) The second diffusion test involved diffusion in space between two parallel plates, to test a situation similar to that encountered at a nmj, ACh molecules start from a point source within a space between two parallel plates, representing axonal and post-synaptic membranes but without secondary folds. This creates a narrow box: the distance between the plates (z dimen-
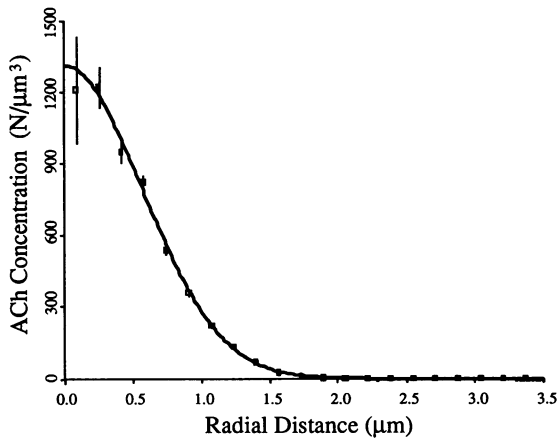
FIGURE 3 Concentration distribution of free ACh molecules diffusing in three-dimensional free space. At time $t = 0$, 5,000 ACh molecules were released from a single point in space. Graph is a snapshot of volume concentration of ACh at varying radial distance from the release point at a time $t = 300$ μs, corresponding to a number $T = 400$ iterations. The mean diffusion length per iteration was $L_d = 0.025$ μm. Concentration equals number of ACh molecules in a bin of radial distance r, divided by the volume of each bin. Smooth curve is theoretically expected result. Points with error bars are Monte Carlo result with Poisson error.

sion of the box, representing the cleft height, Z) is small, about twice the average diffusion step length (L_d), and the length ($2X_{ex}$) and width ($2Y_{ex}$) of the box are each 64 times the height. The two plates are reflecting and the side walls are absorbing (i.e., when a particle comes to the end of the box it is removed from the simulation). The simulation was run for a time t such that $Z \ll (tD)^{1/2} \ll 64Z$. In such a case, when $(tD)^{1/2}$ is large compared with Z, the expected density distribution of A is independent of the z-coordinate (Z) and is given by the two-dimensional function,

$$A(s, t) = (N_0/4\pi tD) \exp(-s^2/4tD), \qquad (9)$$

where $s = (x^2 + y^2)^{1/2}$ is the distance from the origin in the x-y plane alone, and N_0 is the total number of molecules.

The Monte Carlo simulation was used to determine how rapidly the free ACh molecules distribute across the cleft. We see by comparing Figs. 4, a and b, that this occurs by as little as three time steps (2.25 μs). The lateral distribution fits the expected diffusion pattern already after 1 time step (Fig. 4 c) and does not change after three time steps (Fig. 4 d). This attests to our correct choice of each L_j from the Gaussian distribution.

2. Binding and unbinding test

We showed in section II B how to choose Monte Carlo probabilities p_+ and p_- to mimic assumed values of the

binding and unbinding rate constants k_+ and k_- (for single receptor binding sites). We report here on two tests: (a) to test ACh unbinding rate, all AChR were bound at time $t = 0$ and, during the run, p_+ was set to 0 (i.e., no rebinding could occur). The Monte Carlo simulation (Fig. 5 a) then verified that the number of bound receptors decayed exponentially with time $\propto \exp(-k_- t)$ as they should; (b) to test fluctuations at equilibrium, a certain number, N_R of unbound, and N_{AR} of bound receptors (single bindings only in this test), and a number, N_A of free ACh molecules were introduced into a closed box of volume V at time $t = 0$. Because A is the concentration of ACh, $N_A = AV$. For chosen values of k_+ and k_-, the bindings and unbindings in a Monte Carlo run gave values of N_R, N_{AR}, and N_A varying with time but with $N_R + N_{AR}$ equal to the constant number of AChR sites and $N_A + N_{AR}$ equal to the constant number of ACh molecules. The equilibrium values of N_R, N_{AR}, and A (denoted by subscript eq) should be related by

$$[A]_{eq}(N_R/N_{AR})_{eq} = k_-/k_+. \qquad (10)$$

Fig. 5 b shows that deviations of N_{AR} from the equilibrium value $(N_{AR})_{eq}$ fluctuated about zero (as a function of time, after any transient has died down) and that the RMS average of the deviation agreed with Poisson statistics. This demonstrates that the Monte Carlo simulation will correctly mimic expected fluctuations around binding equilibria after an initial transient.

III. MINIMUM STEP LENGTHS AND THE PROBABILITY FOR REBINDING.

When evaluating the Monte Carlo method for obtaining chemical kinetic parameters, two related questions are: (a) what ambiguities might there be in any definition of the unbinding rate constant k_-; and (b) to what extent do we introduce errors by using time and length steps (Δt and L_d) that are larger than those in molecular Brownian motion.

To answer these questions we need to decide the minimum distance $L_{d,min}$ that an ACh molecule must move before the Monte Carlo method can deal with it as being unbound. Recall that Monte Carlo simulations are based on the assumption of random walk, i.e., that there is no correlation in direction of motion from one time step to the next, from which it follows that Δt is proportional to L_d^2 (see Eq. 4). The random walk procedure is justified when time steps are larger than correlation times in the so-called "solvent cage effect" (Koenig and Fischer, 1973; Adelman, 1987). In the solvent cage, provided by the surrounding water (and other) molecules, an ACh molecule would oscillate
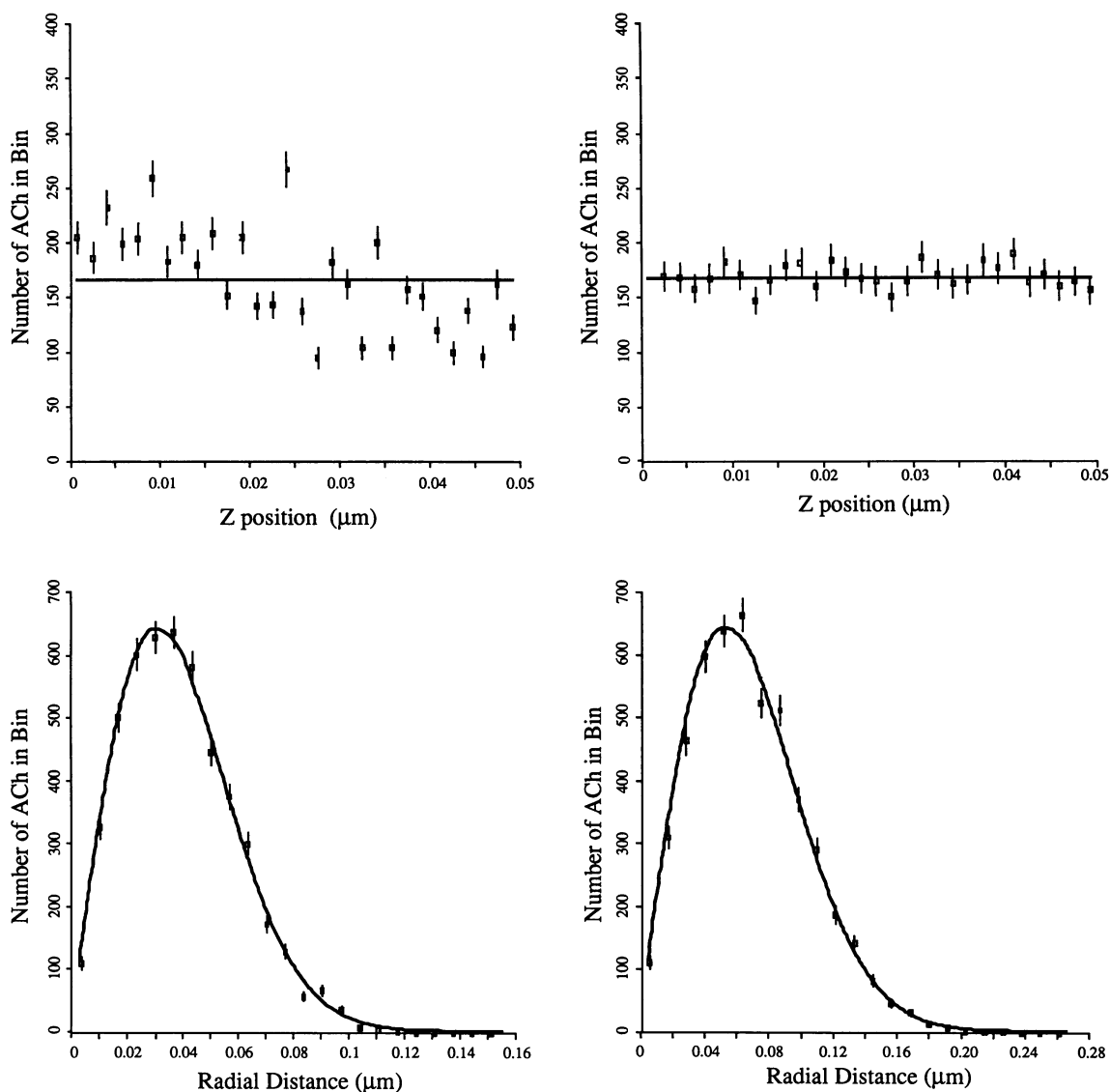
FIGURE 4 (a) Z distribution of the number of free ACh molecules diffusing across the primary cleft (z direction) at a single instance in time after one iteration ($T = 1, t = 0.75$ μs). The cleft is described as a space with reflecting walls at $z = 0$ μm (i.e., axonal membrane) and at $z = 0.05$ μm (i.e., synaptic membrane) divided into 30 bins of height 0.0017 μm each. At time $t = 0$, 5,000 ACh molecules were released at $z = 0$ μm. The data points (□) are numbers of molecules with Poisson error bars per z-bin. The mean diffusion step length was $L_d = 0.025$ μm. The horizontal line represents a uniform distribution of the 5,000 ACh molecules across the 30 bins (i.e., 167 molecules per bin). (b) Z distribution of the number of free ACh molecules, as in Fig. 4 a, but after the third iteration ($T = 3, t = 2.25$ μs) by which time they have reached uniform distribution. (c) Radial distribution of the number of free ACh molecules diffusing in the primary cleft with reflecting walls (at $z = 0$ and $z = 0.05$ μm) after one iteration ($T = 1, t = 0.75$ μs, as in Fig. 4 a). Absorbing walls at maximum radial distance $r = 1.6$ μm. The data points (□) are from the Monte Carlo simulation (with Poisson error bars). The smooth curve is the theoretically expected result. (d) Radial distribution of the number of free ACh molecules as in c, but after the third iteration ($T = 3, t = 2.25$ μs, same time as for Fig. 4 b).

(with a period of order 10^{-12} s and an amplitude of a fraction of 1 nm). Estimates in the literature for solvent cage correlation times tend to be <1 ns. Therefore the smallest Δt (Δt_{min}) for which random walk certainly would apply is of order 1 ns. For the macroscopic diffusion constant $D \sim 6 \times 10^{-6}$ cm²s⁻¹ given for ACh in

the neuromuscular cleft (Eccles and Jaeger, 1958; Krnjevic and Mitchell, 1960; Land et al., 1980, 1981, 1984), a Δt of 1 ns corresponds to an average step length L_d of 1 nm (see Eq. 4). We will therefore define this distance to be $L_{d,min}$. This $L_{d,min}$ is about equal to three diameters of a water molecule and therefore larger than the distance
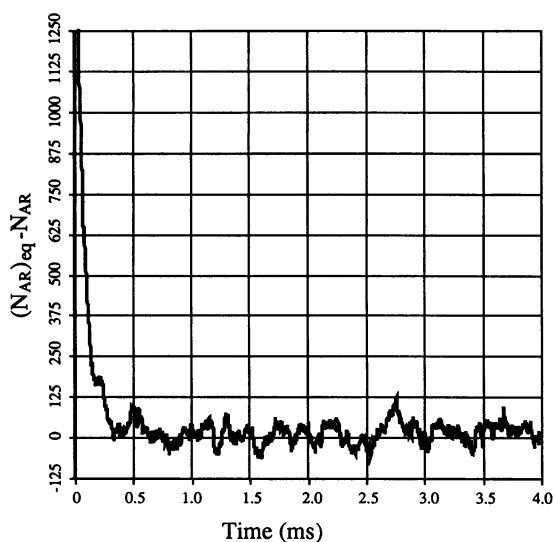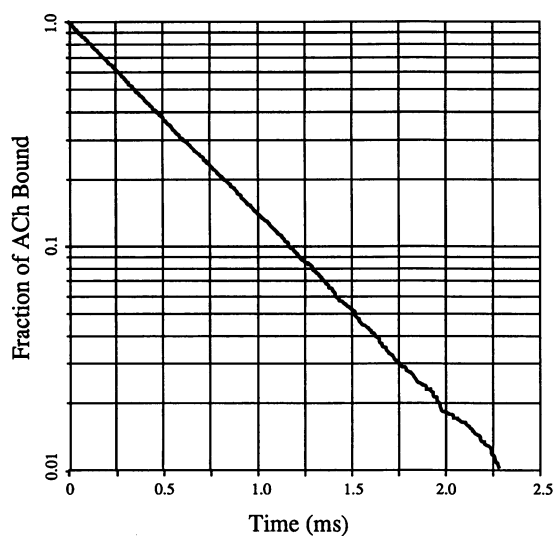
FIGURE 5 (a) Fraction of ACh remaining bound to AChR vs. Time (in unbinding test). At time $t = 0$, all 5,000 ACh molecules were bound to AChR sites. Dark line is the Monte Carlo simulation result for residual bound ACh with an expected e-fold fall time of 0.5 ms. Each iteration was 0.75 μs and k_- was 2,000 s^{-1}. (b) Difference between the actual number of bound molecules, N_{AR}, and the theoretical value expected at equilibrium as given by Eq. 10 ($[N_{AR}]_{eq} = 2,500$) plotted vs. time. At time $t = 0$, 5,000 free ACh molecules were released (i.e., N_{AR} was zero and far from the equilibrium value). The rapid transient in the curve illustrates the capacity of the receptors to bind ACh. Theoretically N_{AR} should approach equilibrium with an exponential relaxation time of 71 μs as observed in this example. As expected, RMS fluctuations of ±5.4 molecules were seen after equilibrium was reached.

for escaping from one cage into another. Although there is some uncertainty about the exact times, and therefore the distances that are involved, one can consider that once a molecule has escaped from a cage it has lost

memory of where it started from, and is therefore moving with random walk motion. Thus the Monte Carlo method would apply to times and distances in the order of 1 ns and 1 nm, respectively. Note also that $L_{d,min}/\Delta t_{min}$ is ~200 times smaller than the thermal speed of an ACh molecule at room temperature in vacuum. Thus, the cage effect slows diffusion, and gives a minimum dimension for noncorrelated random walk.

As stated above, we will consider that an ACh molecule has unbound from an AChR site once it has moved a distance L_d, which must be at least 1 nm (or $L_{d,min}$), from that AChR site. The resultant unbinding rate constant for Monte Carlo simulation will be called k_{-MC}. The difference between k_{-MC} and values obtained by bulk kinetic equations (k_{-bulk}), is largest when the molecules are far from equilibrium. Consider that at an initial time, $t = 0$, all receptors on the membrane are fully bound, and there are no free ACh molecules above the membrane. During a relatively short time, t, (where 1 ns $\ll t \ll$ 10 μs $< 1/k_-$), little free ACh builds up and few AChR binding sites are available. However, the AChR molecule from which the ACh has just unbound and moved away from (i.e., to the defined distance L_d) is, by definition, available. Therefore k_- depends on the probability (f_{reb}) that the ACh rebinds before it has escaped from the vicinity of the AChR from which it unbound. In a bulk chemical kinetics treatment (e.g., by the differential equations used by Land et al., 1981, 1984), the rate equations account for binding of ACh molecules to AChR's only under the assumption that there is no special relationship between a free ACh molecule and the state of a nearby receptor. The increased transient rebinding probability (f_{reb}) is therefore seen as a decreased unbinding rate in the bulk scheme (k_{-bulk}). Thus k_{-bulk} is equal to $k_{-MC}(1-f_{reb})$. Nearer to equilibrium, f_{reb} is compensated for by binding to nearby sites, and k_{-bulk}/k_{-MC} will approach unity.

We will define and calculate f_{reb} in terms of another quantity, n_{ret}, using our Monte Carlo scheme. Recall that in this scheme we represent the membrane area which contains an average of one AChR molecule (with two binding sites) as a square tile of dimension $sq_r = \sigma_r^{-1/2}$. For the lizard nmj this is ~11 nm. We define n_{ret} as the average number of times that a molecule returns to hit the same AChR square before hitting another square (or escaping). Therefore f_{reb} equals n_{ret} times the binding probability per hit (p_+). To obtain a value for n_{ret} by our Monte Carlo method, a single ACh molecule was released from a random spot on one particular receptor square sq_r and, by our definition of unbinding, it was moved away from the membrane a distance L_d. The molecule was allowed to diffuse with average step length L_d, hit the same or another square or to escape, but was not allowed to bind in this simulation. For $L_d = L_{d,min} = 1$

nm and for sq_r = 11 nm we found n_{ret} ~ 1.5. To answer question *b* above, we also carried out a more extensive set of simulations. This was to deal with practical Monte Carlo runs where, to save computer time, we usually use much larger time and average length steps than $L_{d,min}$ (typically Δt ~ 1 μs and L_d ~ 30 nm; about three times larger than the tile size sq_r). Because n_{ret} depends only on the ratio of the average step length L_d used, to the dimension of a AChR tile sq_r, we carried out the calculation for 10 widely different values of L_d/sq_r, each repeated 1,000 times. We thus obtained accurate average values for how n_{ret} depends on L_d/sq_r which is plotted in Fig. 6.

According to Eq. 6, the binding probability per hit (p_+) in a Monte Carlo simulation is proportional to L_d. The expression $f_{reb} = (n_{ret})(p_+)$ can then be rewritten as:

$$f_{reb} = [(L_d/sq_r)n_{ret}]p_{+0}, \tag{11}$$

where p_{+0} is the Monte Carlo binding probability for the special step length $L_d = sq_r$. Fig. 6 shows how f_{reb} depends on step length by plotting the combination $(L_d/sq_r)n_{ret}$ against the ratio L_d/sq_r. The most important result in Fig. 6 is the fact that $(L_d/sq_r)n_{ret}$ (and therefore, from Eq. 11, f_{reb}/p_{+0}) approaches a constant value of ~0.14, when the diffusion length is small ($L_d < 0.2sq_r$). For the molecular motion with $L_{d,min}$ (i.e., 1 nm) the ratio L_d/sq_r is indeed small (~1/11), and, from Eq. 11, f_{reb} is close to 0.14p_{+0}. For the rate constant k_+ at the nmj, derived by us (Land et al., 1980, 1981, 1984) p_{+0} is about 0.01 (see section II B). Thus 0.14 p_{+0} ≪ 1 and the k_- values obtained by
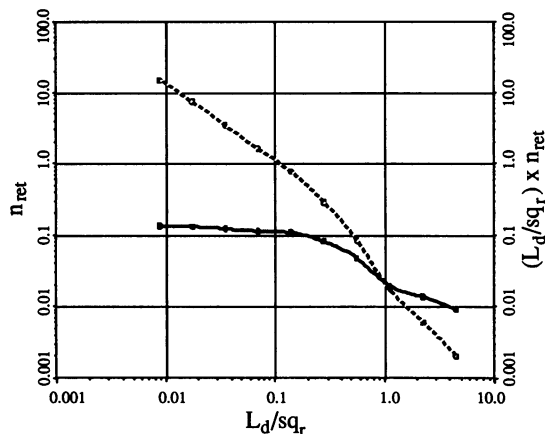
Monte Carlo methods (k_{-MC}) is essentially the same as that obtained by differential equations (k_{-bulk}).

Fig. 6 also shows that $(L_d/sq_r)n_{ret}$, and thus the corresponding value of f_{reb}, further decreases as L_d is increased. Thus $(1-f_{reb}) = k_{-bulk}/k_{-MC}$, is close to unity under all circumstances, and, no major error is introduced in our Monte Carlo simulations, even when L_d is chosen larger than sq_r. Also, since all the dimensions that we deal with in the neuromuscular junction, including the average distance between AChR molecules, are considerably larger than $L_{d,min}$, correlated events from solvent cages do not interfere with the validity of the Monte Carlo simulation for obtaining kinetic parameters of ACh binding and diffusion.

IV. GEOMETRIC CONSIDERATIONS AND ILLUSTRATIVE MODEL RUNS

A. Saturated disk model

To understand possible interpretations of geometric effects on model MEPC's, we should consider the saturated disk model (Matthews-Bellinger and Salpeter, 1978; Salpeter and Land, 1980; Salpeter, 1987). In that model two areas are defined. The first, a_q, is the post-synaptic area containing the number of AChR binding sites equal to the number (N) of ACh molecules in a quantal packet ($a_q = N/\sigma_s$, where σ_s is AChR binding site density). The second, a_e, is the post-synaptic area effectively activated by a single ACh quantum. As a released quantal packet of ACh diffuses and spreads over the post-synaptic membrane it binds AChR binding sites, saturating a small post-synaptic disk area (Fig. 7, *a* and *b*). However, not all the AChR molecules in area a_e are doubly bound or saturated by ACh. In effect only in a central region of a_e are most of the AChR's doubly bound, leaving a predominantly mono-liganded rim. As a_e approaches a_q in size, the ratio of doubly to mono-liganded AChR's increases and more of a_e becomes part of the saturated disk. If we can consider only the doubly liganded AChR's as opening channels (but see section II A), the efficiency of channel opening and thus the amplitude of a MEPC depends on the ratio of doubly liganded to mono-liganded AChR's and thus $a_q/(a_e - a_q)$. This ratio in turn depends on the ratio of diffusion time, a_q/D, to the binding time (t_b): the larger a_q/Dt_b is, the greater is the efficiency.

When AChE is active in the nmj, ACh molecules are hydrolyzed almost immediately after unbinding from AChR. They rarely have a chance to rebind. Double binding to the same AChR is even rarer. The fall time of a MEPC in the presence of AChE, therefore, is approximately equal to $1/\chi_{eff}$. However, when AChE is inactive, ACh can bind AChR, unbind, diffuse, and bind again

FIGURE 6 The dashed curve gives the quantity n_{ret} (left axis), the "average number of returns" as defined in section III, and the solid curve gives the combination $(L_d/sq_r) \times n_{ret}$ (*right axis*) which is proportional to f_{reb} (Eq. 11). Both are plotted against the mean diffusion length L_d in units of sq_r, the length of a "receptor tile."
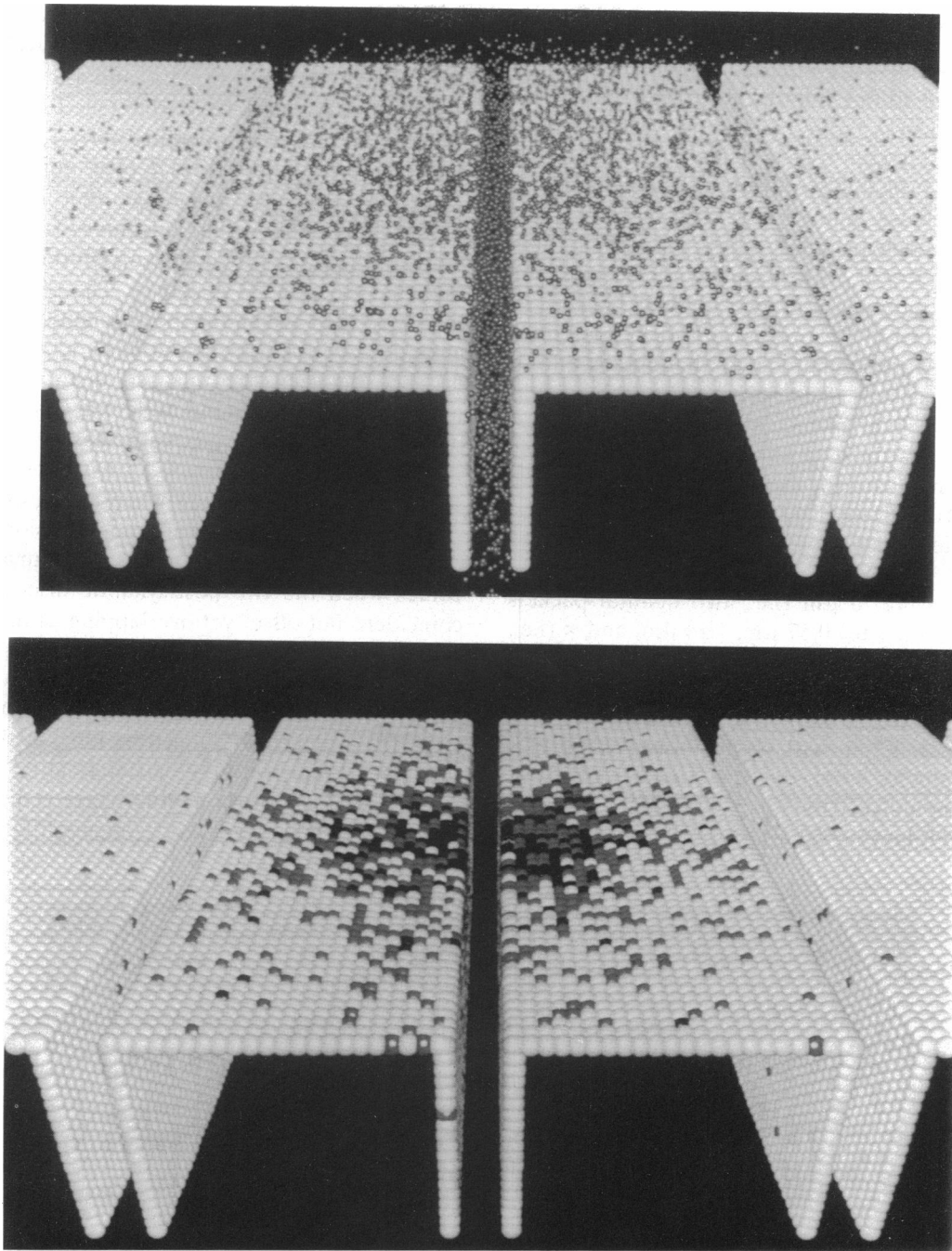
FIGURE 7 (*a, b*) A Monte Carlo simulated nmj with junctional folds (AChE inactive) 30 μs after release of 9,500 ACh molecules showing (*a*) diffusing ACh (*gray points*) and (*b*) post-synaptic response of AChR (unliganded AChR's are white, singly liganded AChR's are gray, and doubly liganded AChR's are black). The axonal membrane and nonreceptive membrane of the bottom of the folds are invisible for illustrative purposes.

many times before diffusing out of the cleft by a process called "buffered diffusion" (Katz and Miledi, 1973; Cull-Candy et al., 1980; Land et al., 1984) which lengthens the MEPC fall time. The a_q/Dt_b ratio affects the extent of buffered diffusion and hence the fall time when esterases are inactivated. The larger a_q/Dt_b is, the longer is the fall time. These considerations affect the interpretations of events when more than one quantal packet is released into the cleft and when folds are added to a nmj.

B. MEPC potentiation

If two quantal packets are released simultaneously and they are adjacent to one another each will activate an area a_e on the post-synaptic membrane. If two release sites are close enough together these a_e areas will overlap and the probability of forming doubly liganded AChR's will increase. Since fewer ACh molecules are then wasted on singly liganded AChR's, potentiation is expected (Hartzell et al., 1975) (see Fig. 8). We used our Monte Carlo simulation with two quantal packets to observe quantitatively the process of MEPC potentiation (the results were compared with that obtained for a single quantal packet). Two 50-nm spherical quantal packets of 9500 ACh molecules each were released simultaneously at varying distances from one another. The simulated nmj used for these model runs contained secondary folds as in the lizard nmj (~ 0.3 μm separation). The release site for each packet was always centered over the mouth of a secondary fold. The distances used were: 0 μm (i.e., two quantal packets released from same site) 0.57 μm, 1.14 μm, and ∞ (i.e., equivalent to two independent quantal packets with no potentiation). Thus in all these cases two packets are summed. The simplified kinetic scheme was used with the following parameters with and without AChE: $\sigma_r =$ 8,200 μm^{-1} (Salpeter et al., 1984), $\sigma_e = 3,500$ μm^{-1} (M. M. Salpeter, unpublished data), $k_{-e} = 3,600$ s^{-1} (Vigny et al., 1978). The following values, $k_{+e} = 5.2 \times 10^7$M^{-1}s^{-1},

$k_{+1} = k_{+2} = 2.6 \times 10^7$M^{-1}s^{-1}, $k_2 = 4,120$ s^{-1}, $\chi_- = 824$ s^{-1}, $D = 6.5 \times 10^{-6}$cm^{2}s^{-1}, and $N = 9,500$ ACh molecules, were preliminary best fit data, and are within the error ranges of values reported earlier (see Land et al., 1984).

Potentiation is quantified in Tables 1, a and b. Whenever the post-synaptic areas a_e overlapped, potentiation could be seen, i.e., responses that exceeded those produced by 2 nonoverlapping quanta (as with ∞ separation). In the case of the peak current the results were as expected (section IV A above). The greatest potentiation was seen when the post-synaptic areas a_e overlapped (as with 0 μm separation) and decreased as the distance between the released quanta increased. At infinite distance the amplitude was exactly twice that obtained from a single quantal release.

During the falling phase (t_f) greatest potentiation was seen, under our conditions when esterases were inactivated, and thus when buffered diffusion could take place. Under those conditions the surprising result comes when the two post-synaptic disc areas are not coincident but offset yet overlapping as in the 0.57 and 1.14 μm separation giving a dumbell-shaped post-synaptic response area. The fall time t_f does not decrease steadily with increasing separation between the release sites, but remains prolonged as long as there is some overlap (possibly with the maximum at 0.57 μm separation). The *shape* of the falling phase is also of interest because one might expect a rapid amplitude decrease at
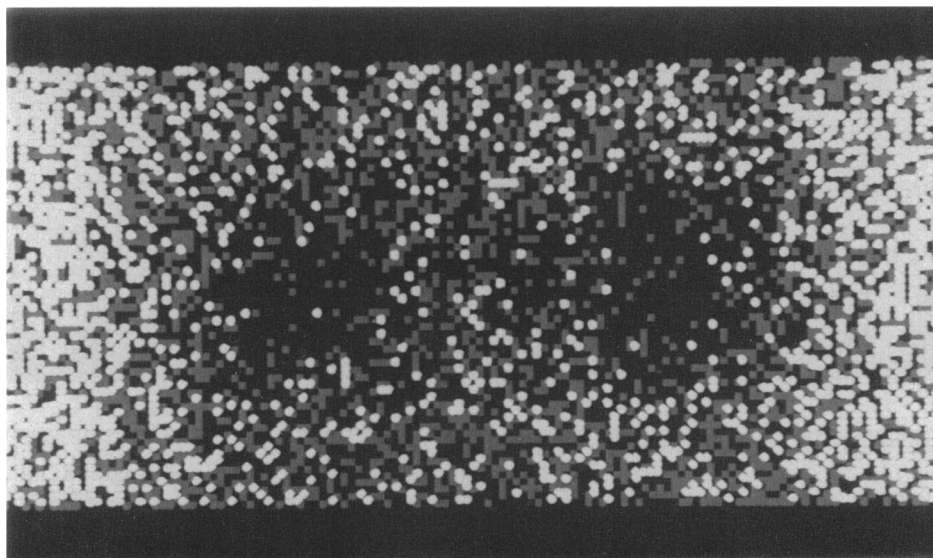

FIGURE 8 Potentiated post-synaptic response for two quantal packets of ACh (N = 9,500 each) released 0.57 μm apart. For clarity, secondary folds are absent. As in Fig. 6 black, gray, and white spheres represent doubly liganded, singly liganded, and unliganded AChR's respectively. AChE is inactive. Note that the overlap of the monoliganded rims (*gray*) of the two spreading saturated disks has lead to an increase in doubly liganded AChR's (*black*) in the region immediately between the disks giving a dumbell-shaped doubly liganded area.

TABLE 1 MEPC potentiation by simultaneous release of two quantal packets

Release spacing	Peak current	t_r	t_f
(a) AChE active			
μm	nA	μs	ms
0	14.3 ± 0.1	72 ± 2	1.41 ± 0.03
0.57	12.2 ± 0.2	69 ± 3	1.39 ± 0.02
1.14	11.3 ± 0.2	62 ± 1	1.38 ± 0.02
∞	11.0 ± 0.2	61 ± 2	1.33 ± 0.03
(b) AChE inactive			
0	19.4 ± 0.2	107 ± 2	5.04 ± 0.1
0.57	17.1 ± 0.2	103 ± 5	5.47 ± 0.2
1.14	15.3 ± 0.2	96 ± 5	5.08 ± 0.2
∞	14.8 ± 0.04	93 ± 6	3.99 ± 0.08

The results of releasing two quantal packets of ACh simultaneously at varying distances from one another are shown for simulated MEPC's with *(a)* and without *(b)* AChE. Release site spacings were 0 μm (i.e. double quantal packet released from same site), 0.57 μm, 1.14 μm, and ∞ μm (i.e. two independent packets whose amplitudes sum linearly without potentiation).Muscles contained junctional folds with spacing as in the lizard nmj and release sites were directly over the mouth of a junctional fold. t_r is 20–80% rise time, and t_f is *e*-fold fall time.

first for the larger separations, followed by a slower decrease when the spreading packets overlap. An example of such a "nonexponential kink" was reported by Hartzell et al. (1975), but is not seen in our simulations: in Fig. 9 the two-quanta MEPC's for three different separations are superposed after normalizing to allow comparison of the shapes. Each of the three curves shows an almost pure exponential falling phase.
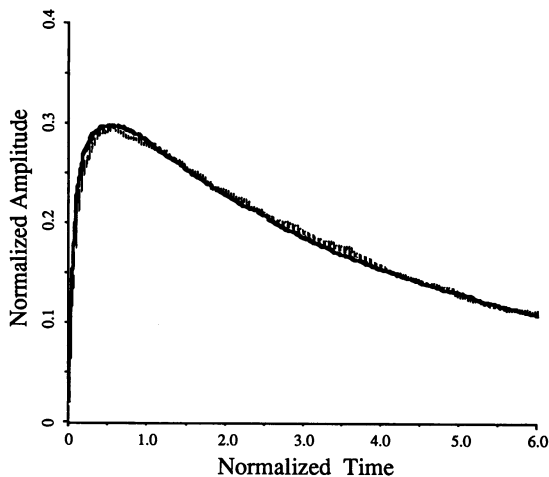
FIGURE 9 Shape of MEPC's for three conditions of potentiation (1.14 μm [——], 0.57 μm [ʷʷ], and ∞ [ᵐᵐ] spacing) normalized in amplitude and fall time to the 1.14 μm spacing case (AChE inactive). The plot illustrates that the normalized shape of three MEPC's is identical and has not been influenced by potentiation.

C. Effects of junctional folds

Different neuromuscular junctions have different amounts of junctional folds varying in depth and spacing (for review see Salpeter, 1987). In the nmj of frog cutaneous pectoris muscle folds are ∼1 μm apart while in that of intercostal muscle of lizard they are ∼0.3 μm apart (Matthews-Bellinger and Salpeter, 1978; Salpeter et al., 1984). In addition, in the frog there is a proximo-distal gradient of post-junctional fold spacing and fold length (in *y*-axis across the primary cleft) (Tremblay et al., 1989). Synapses of the central nervous system contain no secondary folds. The effect of these geometric differences on synaptic kinetics is unknown. We applied our Monte Carlo model (Fig. 10, *a* and *b*) to study the effect of secondary folds on MEPC generation. We initially used three conditions: *(a)* no folds, *(b)* folds as in the lizard twitch fibers with ∼0.3 μm spacing and 0.8 μm depth (AChR down to 0.25 μm), and *(c)* folds as in the frog twitch fibers with ∼1 μm spacing and 0.5 μm depth (AChR down to 0.25 μm). In our initial tests we set the exit half-lengths at $X_{ex} = Y_{ex} = 1.6$ μm and the primary cleft height, Z, to 50 nm. Using these geometric parameters meant that case *b* above had nine folds spread in the primary cleft, but case *c* had only three folds. The folds were arranged parallel to one another at right angles to the long axis of the muscle. In all cases, the same kinetic input parameters for the simplified scheme of Eq. 2 were used as given in section IV B. The packet was released in the primary cleft over the center of a junctional fold (if folds were present).

Tables 2, *a* and *b*, give the results for peak current (A_c), rise time (t_r), and fall time (t_f) for the three cases with and without AChE. We see that both t_r and A_c decrease as more secondary folds are added. This effect of the folds could be understood as follows: wherever a fold is present, some of the ACh molecules are removed from the primary cleft into the secondary cleft. In effect this functions as if there were two or more smaller quantal packets acting on adjacent, overlapping areas (primary cleft plus one, two, or three folds) (see Fig. 7, *a* and *b*, and Fig. 10). As can be seen from the discussion in section IV A above, during the rising phase, the quantal packet has to diffuse far enough to encounter and bind to free AChR binding sites. As the quantal packet is divided between the primary and secondary clefts a_q also decreases and, since efficiency decreases as a_q/Dt_b, so does the amplitude. This effect is accentuated by the additional circumstance that the AChR site density is twice as large in the secondary folds (both surfaces are covered), so that the area (a_q) and thus diffusion time is even smaller. A smaller a_q also means there is a lower probability of overlap between saturated
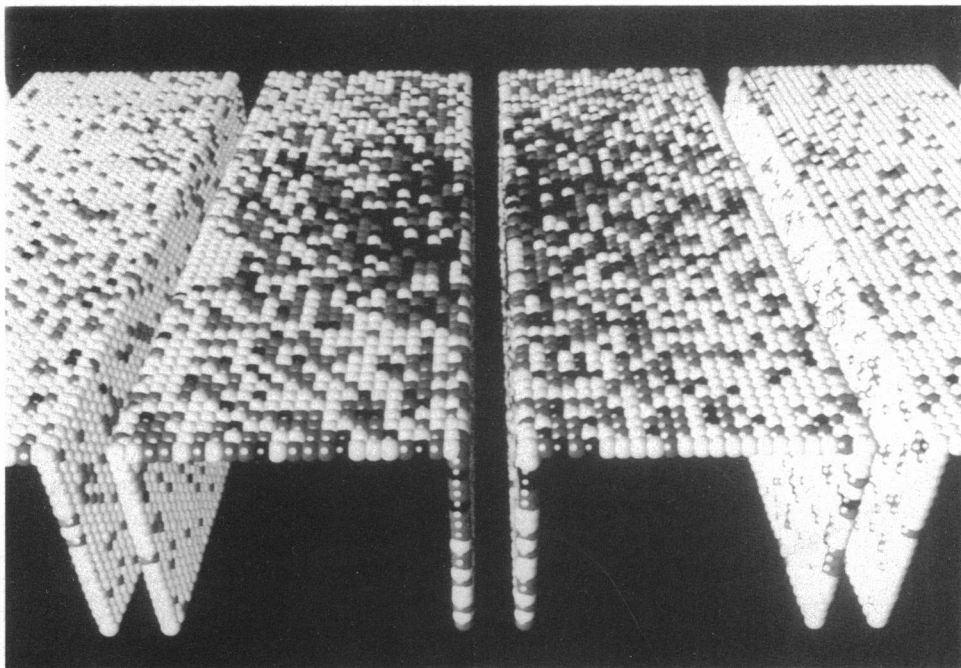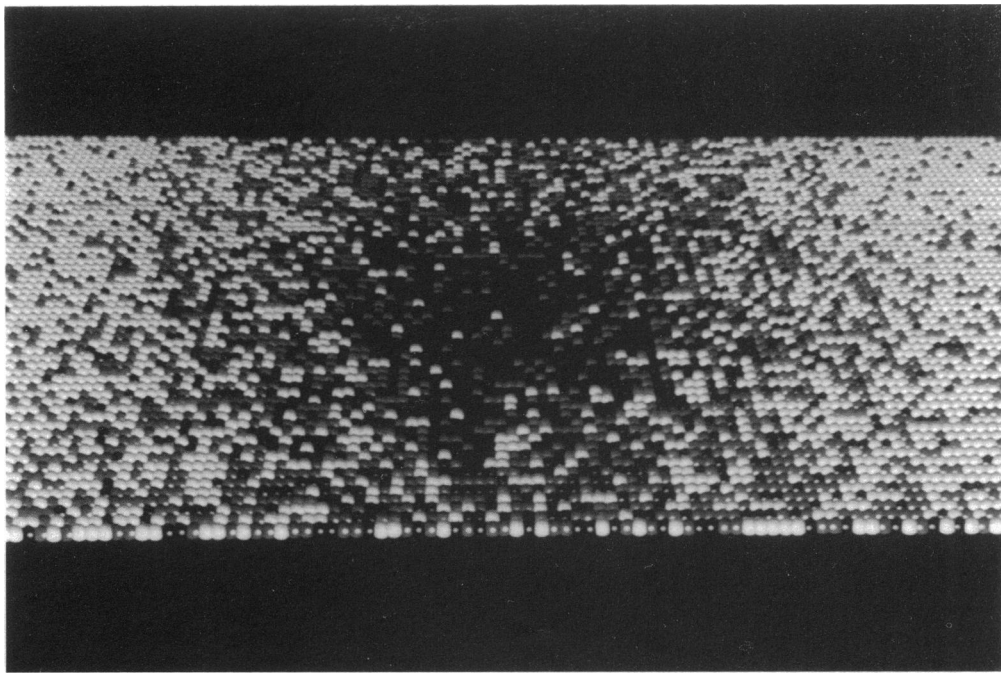
FIGURE 10 (a, b)   Post-synaptic response in the absence (a) and presence (b) of junctional folds (AChE inactive). As in Fig. 7, doubly liganded, singly liganded, and unliganded AChR's are represented by black, gray, and white spheres respectively. At time $t = 0$, 9,500 ACh molecules were released from a single quantal packet in both a and b. With folds present (b), the diffusing ACh packet is divided between the primary and secondary clefts and efficiency of binding to AChR is reduced (see section IV C). Note the much larger doubly liganded (black) region in a as compared with b.

disks resulting from the release of multiple quanta (as would occur during an endplate current [EPC] caused by nerve stimulation). Values for quantal content range from 50–300 (Salpeter, 1987). Thus a smaller a_q leads to

less potentiation of the current amplitude (see section IV B) and a more linear response to multiple quanta.

We can make some rough estimates for the currents produced in a full EPC, i.e., after the simultaneous

TABLE 2 Effect of varying secondary fold spacing on MEPC wave form

Fold spacing	Fold depth	Peak current	t_r	t_f
		(a) AChE active		
μm	μm	nA	μs	ms
No folds	0	7.36 ± 0.09	87 ± 3	1.43 ± 0.02
1.0	0.5	6.29 ± 0.1	73 ± 3	1.45 ± 0.09
0.29	0.8	5.48 ± 0.1	61 ± 2	1.33 ± 0.03
		(b) AChE inactive		
No folds	0	9.98 ± 0.15	120 ± 4	3.99 ± 0.09
1.0	0.5	9.27 ± 0.17	121 ± 5	4.26 ± 0.12
0.29	0.8	7.38 ± 0.04	93 ± 6	3.99 ± 0.08

The results for three different fold spacings are shown: no folds; 1.0 μm spacing (as in the frog); and 0.29 μm (as in the lizard). Results are shown for MEPC's simulated with AChE active (a) and AChE inactive (b). t_r is 20–80% rise time, and t_f is e-fold fall time.

release of 50–300 quantal packets of ACh. If the release sites were randomly distributed over the entire endplate, the average separation between adjacent release sites would be larger than 2 μm. However, with fold geometry roughly as in the lizard nmj and with AChE active, Table 1 a shows that potentiation is unimportant when the separation of adjacent release sites exceeds 0.6 μm. Therefore, a linear response (absence of potentiation) should hold for quantal contents appreciably larger than the usual 50–300 even if there were no folds, but would extend to an even greater number of quanta if there were folds. Given the geometry and size of the nmj (Matthews-Bellinger and Salpeter, 1978) and reported quantal contents, we conclude that the effect of the folds on the linearity of a full EPC is relatively unimportant. It seems likely that the folds primarily have a different function, as for example in facilitating the replenishment of Na$^+$ ions.

The effect of secondary folds on the fall time is puzzling however. With AChE present, the falling phase mainly represents unbinding (because little rebinding of released ACh molecules occurs) (Anderson and Stevens, 1973), and folds should make no difference. However, when AChE is inactivated, there is considerable rebinding, followed by further binding (i.e., buffered diffusion). Such buffered diffusion should go on for a shorter period when folds are present because both N and $a_q/(a_e - a_q)$ are smaller. Yet this is not the case and the fall time is relatively unaffected. This result emphasizes that, as in the case of the dumbell-shaped post-synaptic area during potentiation, when complex geometries are involved, the effective buffered diffusion is difficult to predict analytically and needs the Monte Carlo method to determine empirically.

In conclusion, the presence of folds decreases the efficiency of ACh binding. This would result in lower

amplitude MEPC's unless the kinetic parameters were altered in such junctions to compensate for the lower efficiency. Modeling kinetic parameters to fit experimentally obtained MEPC's for different species and junctional geometry will be the subject of a subsequent paper.

D. Proximodistal gradient in frog muscle

Robitaille et al. (1987) have observed a proximodistal decrease in the amplitude of miniature endplate potential (MEPP) in the frog cutaneous pectoris muscle. This gradient parallels a proximodistal gradient in post-junctional geometry in which the spacing between folds increases (i.e., fewer folds) and the side to side length of the post-junctional fold ($2Y_{ex}$, at right angles across the cleft) decreases, (i.e., the junction gets narrower) (Tremblay et al., 1989). From the above argument (section IV C) one would assume that increasing the junctional fold-to-fold spacing should increase MEPC amplitude. However, the shorter width of the folds ($2Y_{ex}$) across the primary cleft shortens the distance before ACh molecules diffuse out of the cleft. We have used the Monte Carlo simulation with the following geometric parameters as given by Tremblay et al. (1989): junctional fold width ($2Y_{ex}$), 3.0 μm proximal, and 1.5 μm distal, and junctional fold spacing, 0.5 μm proximal, and 1.0 μm distal. We found that even with AChE intact, MEPC amplitude (A_c) and fall time (t_f) were slightly lower ($\sim 10\%$) in the distal segment (see Tables 3, a and b). In the absence of AChE, MEPC amplitudes were ~ 1.3 times lower and t_f was ~ 2.8 times shorter in the distal compared with the proximal segment. Our results are consistent with those seen by Tremblay et al. (1989) in which peak miniature end plate potential (MEPP) amplitudes were ~ 3 to 5 times lower distally. (The MEPP amplitude is expected to be roughly the MEPC amplitude times t_f neglecting the effect of the membrane time constant). We, however, differ from Tremblay et al.

TABLE 3 Effect of proximodistal gradient in fold geometry on MEPC wave form

Fold spacing	Fold length ($2Y_{ex}$)	Peak current	t_r	t_f
	(a) AChE active			
μm	μm	nA	μs	ms
0.5 (proximal)	3.0	6.18	71	1.46
1.0 (distal)	1.5	5.76	58	1.33
	(b) AChE inactive			
0.5 (proximal)	3.0	8.91	104	4.92
1.0 (distal)	1.5	6.90	74	1.73

Geometric parameters for proximal and distal nmj segments for frog are as given by Tremblay et al. (1989). Results are shown for Monte Carlo-simulated MEPC's with AChE active (a) and AChE inactive (b).

(1989) in the interpretation of the results. Whereas Tremblay et al. argue that increased fold spacing in the distal segment explains the decreased MEPP amplitude, we find (section IV C) that increased fold spacing *increases* MEPC amplitude. Therefore, the much shorter Y_{ex} in the distal segment is the major factor determining the decreased A_c and t_r.

V. ALGORITHMS FOR SIMPLE VS. FULL KINETIC SCHEMES

The simplified kinetic scheme previously described in Eq. 2 (section II A) simulates the $A_2R_c^*$ state of the receptor complex without explicitly putting in the kinetics of the isomerization step as discussed in section II. This simplified equation is based on the assumption that the rise time (t_r) is short relative to the fall time (t_f) and that the channel opening rate (β) is fast relative to diffusion (D) and binding (k_+). A correction to Eq. 1 can compensate for the extent to which these conditions are not fully met (Bartol et al., 1990). However, our Monte Carlo simulation makes it simple to explicitly add an isomerization step so that the full kinetic scheme of Eq. 1 may be implemented. We carried out some Monte Carlo simulations both with the full and with the simplified scheme to compare computing costs and numerical accuracy.

The two computing schemes are identical, except when AChR molecules become doubly bound. For such AChR molecules the full scheme involves an extra choice of a random number to give the probability of whether a channel will open or not. The increase in computing time from the simplified to the full scheme was <10%. This small change in computing costs may seem surprising, but is due to two facts: (*a*) there are relatively few doubly bound AChR complexes compared with freely diffusing AChR molecules. (*b*) For the diffusion routine three random numbers are required (the three spatial dimensions) for each ACh molecule followed by a test for whether and where each molecule crossed a membrane (see section II B), whereas for the isomerization routine only one random number is needed for each of the doubly liganded AChR molecules.

With the full scheme the Monte Carlo simulation of the instantaneous channel current showed more high frequency noise (or flicker) due to channel openings and closings (see Fig. 11). The amplitude of the noise increased as the ratio of α to β approached 1.0 where channel flicker is maximum. This is the expected result from the formula for statistical variance as $p(1 - p)$, which is maximum at $p = 0.5$ (i.e., when $\alpha = \beta$). Channel flicker is a phenomenon which is expected to occur with a real MEPC in the nmj and is simulated by the Monte
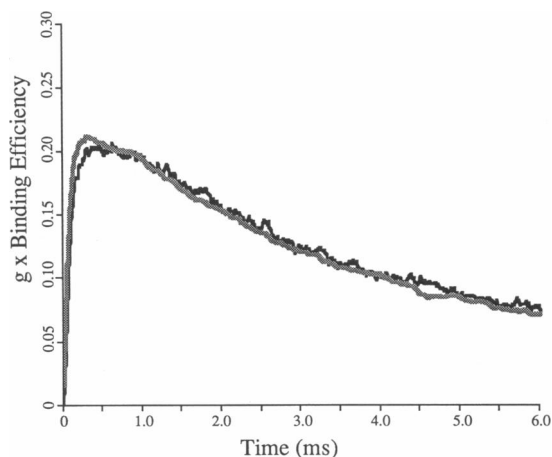

FIGURE 11 Two single MEPC's derived from the full kinetic scheme (Eq. 1) (*black*) and the simplified kinetic scheme (Eq. 2) (*gray*) (AChE inactive). Note that the shapes are similar but that the more realistic full scheme reveals the noise due to multiple channel openings and closings.

Carlo algorithm. Fortunately there are many isomerization steps per rise time and the noise has little affect on the numerical accuracy of the main quantities to be computed. We repeated the same computations a number of times, using different random number seeds, and found that the standard deviations for the peak amplitude, rise time, and fall time was ~5% each, both for the full and the simplified schemes. We found that for conditions expected to prevail at the nmj, and using the kinetic parameters as given in section IV B, results obtained from the simplified and full equation were compatible. Because the simplified scheme is only approximate, and because the increased cost for the full scheme is minimal, the full scheme is preferable whenever Monte Carlo simulation is used. A detailed analysis on when and under what circumstances the results from the two kinetic schemes diverged will be given in a subsequent paper as will the analysis of complex schemes such as singly liganded openings, a third ACh binding site, and nonequivalent binding kinetics (see section II A).

REFERENCES

Adams, P. R. 1975. An analysis of the dose-response curve at voltage-clamped frog endplates. *Pfluegers Arch. Eur. J. Physiol.* 360:145–153.

Adelman, S. A. 1987. Solvent cage effects and the dynamics of liquid state chemical reactions. *In* Reviews of Chemical Intermediates. O. P. Strausz, J. K. S. Wan, and M. C. Depew, editors. Elsevier Science Publishers, B. V., Amsterdam. 321–338.

Anderson, C. R., and C. F. Stevens. 1973. Voltage clamp analysis of acetylcholine produced endplate current fluctuations at frog neuromuscular junction. *J. Physiol. (Lond.).* 235:655–691.

Bartol, T. M., E. E. Salpeter, and M. M. Salpeter. 1990. A comparison of kinetic models of the neuromuscular junction using Monte Carlo simulation. *Soc. Neurosci. Abstr.* 16:673.

Betz, W. J., and B. Sakmann. 1973. Effects of proteolytic enzymes on function and structure of frog neuromuscular junctions. *J. Physiol. (Lond.).* 230:673–688.

Blount, P., and J. P. Merlie. 1989. Molecular basis of the two nonequivalent ligand binding sites of the muscle nicotinic acetylcholine receptor. *Neuron.* 3:349–357.

Crank, J. 1975. The Mathematics of Diffusion. Clarendon Press, Oxford. 414 pp.

Cull-Candy, S. G., R. Miledi, and O. D. Uchitel. 1980. Diffusion of acetylcholine in the synaptic cleft of normal and myasthenia gravis human endplates. *Nature (Lond.).* 286:500–502.

Dionne, V. E. 1976. Characterization of drug iontophoresis with a fast microassay technique. *Biophys. J.* 16:705–717.

Eccles, J. C., and J. C. Jaeger. 1958. The relationship between the mode of operation and the dimensions of the junctional regions at synapses and motor end-organs. *Proc. R. Soc. Lond. (Biol.).* 148:38–56.

Hall, Z., and R. B. Kelly. 1971. Enzymatic detachment of endplate acetylcholinesterase from muscle. *Nature (New Biol.).* 232:62–63.

Hartman, D. S., and T. Claudio. 1990. Coexpression of two distinct muscle acetylcholine receptor α-subunits during development. *Nature (Lond.).* 343:372–375.

Hartzell, H. C., S. W. Kuffler, and D. Yoshikami. 1975. Post-synaptic potentiation: Interaction between quanta of acetylcholine at the skeletal neuromuscular synapse. *J. Physiol. (Lond.).* 251:427–463.

Katz, B., and R. Miledi. 1973. The binding of acetylcholine to receptors and its removal from the synaptic cleft. *J. Physiol. (Lond.).* 231:549–574.

Koenig, T., and H. Fischer. 1973. "Cage" effects. *In* Free Radicals. J. K. Kochi, editor. John Wiley & Sons, New York. 1:157–185.

Krnjevic, K., and J. F. Mitchell. 1960. Diffusion of acetylcholine in agar gels and in the isolated rat diaphragm. *J. Physiol. (Lond.).* 153:562–572.

Labarca, P., M. S. Montal, J. M. Lindstrom, and M. Montal. 1985. The occurrence of long opening in the purified cholinergic receptor channel increases with acetylcholine concentration. *J. Neurosci.* 5:3409–3413.

Land, B. R., W. V. Harris, E. E. Salpeter, and M. M. Salpeter. 1984. Diffusion and binding constants for acetylcholine derived from the falling phase of miniature endplate currents. *Proc. Natl. Acad. Sci. USA.* 81:1594–1598.

Land, B. R., E. E. Salpeter, and M. M. Salpeter. 1980. Acetylcholine receptor site density affects the rising phase of miniature endplate currents. *Proc. Natl. Acad. Sci. USA.* 77:3736–3740.

Land, B. R., E. E. Salpeter, and M. M. Salpeter. 1981. Kinetic parameters for acetylcholine interaction in intact neuromuscular junction. *Proc. Natl. Acad. Sci. USA.* 78:7200–7204.

Matthews-Bellinger, J., and M. M. Salpeter. 1978. Distribution of acetylcholine receptors at frog neuromuscular junctions with a discussion of some physiological implications. *J. Physiol. (Lond.).* 279:197–213.

McMahan, U. J., J. R. Sanes, and L. M. Marshall. 1978. Cholinesterase is associated with the basal lamina at the neuromuscular junction. *Nature (Lond.).* 271:172–174.

Ortega, J. M., and W. G. Poole. 1981. An Introduction to Numerical Methods for Differential Equations. Pitman, Boston. 329 pp.

Robitaille, R., J. P. Tremblay, and G. Grenon. 1987. Non-uniform distribution of miniature endplate potential amplitudes along the length of the frog neuromuscular junction. *Neurosci. Lett.* 74:187–192.

Rubinstein, R. Y. 1981. Simulation and the Monte Carlo Method. John Wiley & Sons, New York. 278 pp.

Salpeter, M. M. 1987. Vertebrate neuromuscular junctions: general morphology, molecular organization, and functional consequences. *In* The Vertebrate Neuromuscular Junction. Alan R. Liss Inc., New York. 1–54.

Salpeter, M. M., and B. R. Land. 1980. Physiological consequences of ACh receptor and esterase distribution in vertebrate endplates. *In* La Transmission Neuromusculaire. Fondation Singer-Polignac, editor. Masson, Paris. 101–110.

Salpeter, M. M., C. D. Smith, and J. A. Matthews-Bellinger. 1984. Acetylcholine receptor at neuromuscular junctions by EM autoradiography using mask analysis and linear sources. *J. El. Micr. Tech.* 1:63–81.

Sheridan, R. E., and H. A. Lester. 1977. Rates and equilibria at the acetylcholine receptor of *Electrophorus electroplaques. J. Gen. Physiol.* 70:187–219.

Sine, S. M., and P. Taylor. 1980. Relationship between agonist occupation and the permeability response of the cholinergic receptor revealed by bound cobra α-toxin. *J. Biochem.* 255:10144–10156.

Torney, D. C., and T. T. Warnock. 1988. Computer simulation of diffusion-limited chemical reactions in three dimensions. *Intl. J. Supercomp. Appl.* 1:33–43.

Tremblay, J. P., R. Robitaille, O. Martineau, C. Labrecque, and M. A. Fahim. 1989. Proximodistal gradients of the post-junctional folds at the frog neuromuscular junction: a scanning electron microscopic study. *Neurosci.* 30:535–550.

Turner, J. S. 1977. Discrete simulation methods for chemical kinetics. *J. Phys. Chem.* 81:2379–2408.

Udgaonkar, J. B., and G. P. Hess. 1986. Acetylcholine receptor kinetics: chemical kinetics. *J. Membr. Biol.* 93:93–109.

van der Laan, C. G., and N. M. Temme. 1984. Calculation of Special Functions: the Gamma Function, the Exponential Integrals and Error-Like Functions. Centrum voor Wiskunde en Informatica, Amsterdam. 231 pp.

Vigny, M., S. Bon, J. Massoulie, and F. Leterrier. 1978. Active-site catalytic efficiency of acetylcholinesterase molecular forms in *Electrophorus, Torpedo,* rat and chicken. *J. Biochem.* 85:317–323.

Wathey, J. C., M. M. Nass, and H. A. Lester. 1979. Numerical reconstruction of the quantal event of nicotinic synapses. *Biophys. J.* 27:145–164.